Numerical Simulations of a 100-kW Class Nested Hall Thruster with the 2-D Axisymmetric Code Hall2De

IEPC-2017-220

Presented at the 35th International Electric Propulsion Conference
Georgia Institute of Technology, Atlanta, Georgia
October 8 – 12, 2017

Ioannis G. Mikellides* and Alejandro Lopez Ortega†
Jet Propulsion Laboratory, California Institute of Technology, Pasadena, CA, 91109, USA

Results from the first numerical simulations of a nested Hall thruster are presented. The X3 is a 100-kW class thruster with three acceleration channels and one center-mounted hollow cathode that will be incorporated in the Aerojet Rocketdyne XR-100 propulsion system currently under development through NASA's Next Space Technologies for Exploration Partnerships (NextSTEP) program. The simulations were conducted with the r-z axisymmetric code Hall2De developed at JPL over the last decade, and focused on operation with all three channels firing, at discharge voltages of 300, 400 and 800 V. The corresponding discharge power levels were 38, 49.6 and 100 kW. A recent experimental campaign conducted at NASA GRC provided measurements of the X3's performance at a wide range of channel combinations and operating conditions including 300 and 400 V. However, the final anode flow rates specified during the test and used as input to Hall2De became available only after the simulations had been completed and therefore an unambiguous one-on-one comparison between computed and measured performance was not possible. In one case, namely 400 V and 49.6 kW, the anode flow rates were the closest between simulation and experiment: 9.6% higher in the simulation for the inner channel and 1.4% lower for the outer channel. For this operating condition results from the simulations and experiments were found to be within 5% for the thrust and anode specific impulse and within 10% for the anode efficiency. The Hall2De simulations also allowed for the first estimates of erosion by ion sputtering. The computed erosion rates along the (BN) channel walls of the X3 were found to be in the order 10^{-3} mm/h (10^{3} μm/kh) at 300 V. The rates at 800 V were a few times higher than those at 300 V.

* Principal Engineer, Electric Propulsion Group, Ioannis.G.Mikellides@jpl.nasa.gov
† Member of the Technical Staff, Electric Propulsion Group, Alejandro.Lopez.Ortega@jpl.nasa.gov

I. Introduction

The X3 Nested Hall Thruster (NHT) is a 100-kW class, three-channel thruster that will be incorporated into the XR-100 propulsion system currently under development through NASA's Next Space Technologies for Exploration Partnerships (NextSTEP) program. NextSTEP encompasses a set of projects aimed at improving small satellites, propulsion and human living quarters in space. The XR-100 project is a collaborative effort between Aerojet Rocketdyne, the University of Michigan (UM), the Jet Propulsion Laboratory (JPL) and the NASA John Glenn Research Center (GRC) that aims to advance a 100-kW integrated Hall Thruster System, which includes the thruster, power processing unit and mass flow controller, to Technology Readiness Level 5.

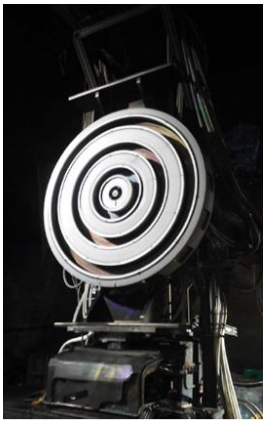

Metric	Design Goals
Specific impulse (s)	2,000-5,000
In-space lifetime (h)	>50,000
Operational lifetime (h)	>10,000
System efficiency (%)	>60
Power per thruster (kW)	250
Specific power (kW/kg)	>0.2

Fig 1. Left: The X3 thruster mounted on a thrust stand at UM. Right: Design goals of NASA's NextSTEP XR-100 project.

The X3 NHT, shown in Fig 1-left, is largely the product of earlier work performed at UM that began several years ago [1-3] in collaboration with the Air Force Research Laboratory, GRC, and JPL. The thruster has an extensive design heritage which includes the development of the X2 NHT [4] and the single-channel high-power Hall thrusters NASA-457M-v1 &v2, NASA-400M, and NASA-300M [5-9]. It was built to employ a center-mounted LaB_6 hollow cathode provided by JPL and three acceleration channels, and to operate at seven distinct operating regimes. The regimes consist of each channel operating individually, all three operating simultaneously, and the various combinations of two. The X3 is designed to operate at discharge powers between 2 and 250 kW, providing up to 15 N of thrust. The required propellant flow rate ranges approximately 5-180 mg/s of xenon. The NHT channels are not magnetically shielded, yet one of the design goals (Fig 1-right) is operational lifetime capability that exceeds 10,000 h. Thus, one of the primary contributions to XR-100 project by JPL was to employ our in-house 2-D (r-z) axisymmetric plasma code Hall2De [10, 11] to assess the life of the thruster. OrCa2D, JPL's 2-D axisymmetric hollow cathode code, has also been employed to assess the life of the LaB_6 cathode. The results from the hollow cathode modeling work will be reported in a future publication. In this paper we present only the results from the Hall2De simulations of the X3, and include limited comparisons with performance measurements at discharge voltages of 300 and 400 V in Sec. III.A. The measurements were acquired during a recent test campaign at NASA GRC and are reported in detail in [12]. A few interesting features from the simulations that are associated with the behavior of the plasma in the near plume region of the thruster are

also discussed in this section. In Sec. II.B we provide predictions of the erosion rates along the channel walls when all three channels are firing at 300 and 800 V. Concluding remarks are provided in Sec. IV. A general description of Hall2De, along with the computational arrangement and boundary conditions (BC) used in the simulations of the X3 are provided in Sec. II.

II. Computational Methods

A. General description of Hall2De and recent advancements

The numerical simulations presented in this paper have been performed with the Hall2De code, a two-dimensional (2-D), axisymmetric computational solver of the conservation equations that govern the evolution of the partially ionized gas in Hall thrusters [10, 11, 13]. The governing equations, numerical methodology, various thruster simulations and comparisons with measurements have been presented elsewhere [10, 14, 15]. Here, we provide only a brief overview for completeness and outline physics and numerical advancements implemented recently in the code, some of which were implemented to allow for the simulation of Hall thrusters operating with more than on acceleration channels.

In Hall2De all governing equations are solved on a magnetic-field-aligned computational mesh (MFAM). The solution of the electron energy conservation equation is obtained semi-implicitly; the thermal conduction and current convection terms are implicit whereas all other terms are evaluated explicitly. Current conservation, incorporating Ohm's law to solve for the electron current density, is also solved implicitly. Ohm's law is solved in the frame of reference of the magnetic field with the electrical resistivity accounting for contributions from collisions of electrons with all other species. It is now widely accepted that transport of electrons in Hall thrusters is driven to a large extent by non-classical mechanisms, possibly by plasma turbulence [16-21]. In numerical simulations this non-classical transport has typically been modeled using an effective or "anomalous" collision frequency. Denoting this collision frequency as ν_α, we impose in Hall2De a so-called transport coefficient function $f_\alpha(r,z)$ and set $\nu_\alpha=f_\alpha\omega_{ce}$ with ω_{ce} denoting the electron cyclotron frequency. Our specification of f_α is guided by plasma measurements whenever they exist. Examples of the empirically-guided anomalous collision frequency in Hall thrusters as implemented in Hall2De has been presented in several articles in the past (e.g. see Ref [22]).

The default approach in Hall2De to obtain the solution of the conservation equations for the heavy species avoids discrete-particle methods. However, an option to invoke the Particle-in-Cell (PIC) method for ions has recently been incorporated in the code (e.g. see [23]). The evolution of the (collision-less) neutral species is computed using line-of-sight formulations that account for their depletion through ionization [11]. If PIC is not invoked, ions are treated as an isothermal, cold (relative to the electrons) fluid, accounting for the drag force and the ion-pressure gradient. The equations of motion for ions are discretized in time using a semi-implicit predictor/multi-corrector [24] scheme. Though relaxation times for ions can be shown to be small enough inside the acceleration channel, such times can become exceedingly high in the near plume region. If modeled as a single fluid, convection of slow ions in the near plume will occur at the mean velocity, which is dominated by the momentum of the fast ions. This would in turn result in erroneously low particle densities in regions that reside outside the main beam. To circumvent this limitation Hall2De employs a multi-fluid algorithm described in more detail in

[13]. Briefly, determination of the fluid to which a given ion belongs is made upon examining the plasma potential at the location where the ion mass element was generated. So-called "threshold" potentials are specified in Hall2De to determine the maximum energy at which each ion population is created. Ions of different populations are created by ionization and charge-exchange collisions depending on how the threshold energy compares to the local value of the plasma potential. In the present simulations we allow for three distinct ion fluids. The second fluid is associated with a threshold potential that is ~80% of the discharge voltage and for the third and slowest-ion fluid the threshold potential is 50 V. The first fluid is always that associated with the ion beam. Up to triply charged ions are also accounted for each of the three fluids yielding a total of nine ion momentum and nine ion continuity equations.

In the majority of the computational domain the assumption of quasi-neutrality in the plasma is valid. Therefore, near most solid surfaces of the thruster, BCs that account for the sheath may be implemented based on a thin-sheath approximation [10]. However, there are some regions near walls where the sheath can become large compared to the local computational cell size. These regions develop typically at the exit of the acceleration channel, in the vicinity of the wall edges where the turning flow undergoes significant expansion. This, in turn, can lead to very low local densities and large Debye lengths. To better model these regions, a space charge algorithm has been developed in Hall2De which solves Poisson's equation to determine the space charge potential in areas near the thruster walls where the local Debye length is larger than the distance from the cell centroid to the nearest wall. The details of the algorithm and representative simulations results are provided in [25]. Since the impact of the space-charge regions is more significant in magnetically shielded thrusters, all simulations presented herein do not incorporate the space charge algorithm.

Recently the code also has been updated to allow for easier implementation of different electrical BCs. This was motivated by recent experimental investigations of different electrical configurations in the H6MS [26] Hall-effect Rocket with Magnetic Shielding (HERMeS) [27, 28]. The updates now allow for insulating, conducting and current-collecting conditions at any of the wall boundaries. At insulators a zero-current condition is imposed and the model for the convective heat losses follows the formulations of Hobbs and Wesson [29]. At conducting boundaries the electron current to the wall is reduced from its random thermal flux value due to the presence of the sheath and the Bohm condition is set as the minimum speed of ions entering the sheath, as described in [30, 31]. For this BC the value of the applied voltage must be specified. For current-collecting boundaries an iteration is performed on the applied voltage until the specified current has been collected. The particle and heat fluxes are determined assuming the boundary is a conductor. If the collected current is zero then the wall is a floating boundary.

B. **Computational arrangement and simulation conditions for the X3 NHT**

Typically the MFAM in Hall2De spans a computational domain in r-z geometry that extends several times the thruster channel length in the axial direction, and encompasses the cathode boundary and the thruster centerline. In the present 3-channel simulations the near-plume computational domain was approximately 20 times the acceleration channel length L in the axial direction and 17 times the outer radius of the outer channel wall. Shown in Fig 2 is a schematic of the computational domain for the X3 NHT simulations with naming conventions of various thruster components and boundaries. The naming abbreviations we follow in this article for each of the three acceleration channels is as follows: Outer acceleration channel is denoted with "O", the middle channel with "M" and the inner with "I".

The conservation equations solved by Hall2De are closed with BCs at all surfaces. Referring to Fig 2, we impose dielectric (electrical insulator) BCs at the outer and inner boron nitride (BN) walls of the acceleration channels. In the X3 the poles are coated with a thin layer of alumina. These poles have therefore been modeled also as dielectric boundaries. The three anodes and the magnetic iron (MI) walls for each acceleration channel are modeled as electrical conductors. Propellant injection is imposed along each boundary between the anode surfaces, as shown in Fig 2, and uses the specified anode flow rates for each channel to define the mass flux there. At the cathode boundary the neutral particle flux, ion flux, plasma potential and electron temperature are specified. The far plume solution is subject to outflow BCs as shown in Fig 2-right along which a zero-current condition and a fixed electrons temperature are imposed.

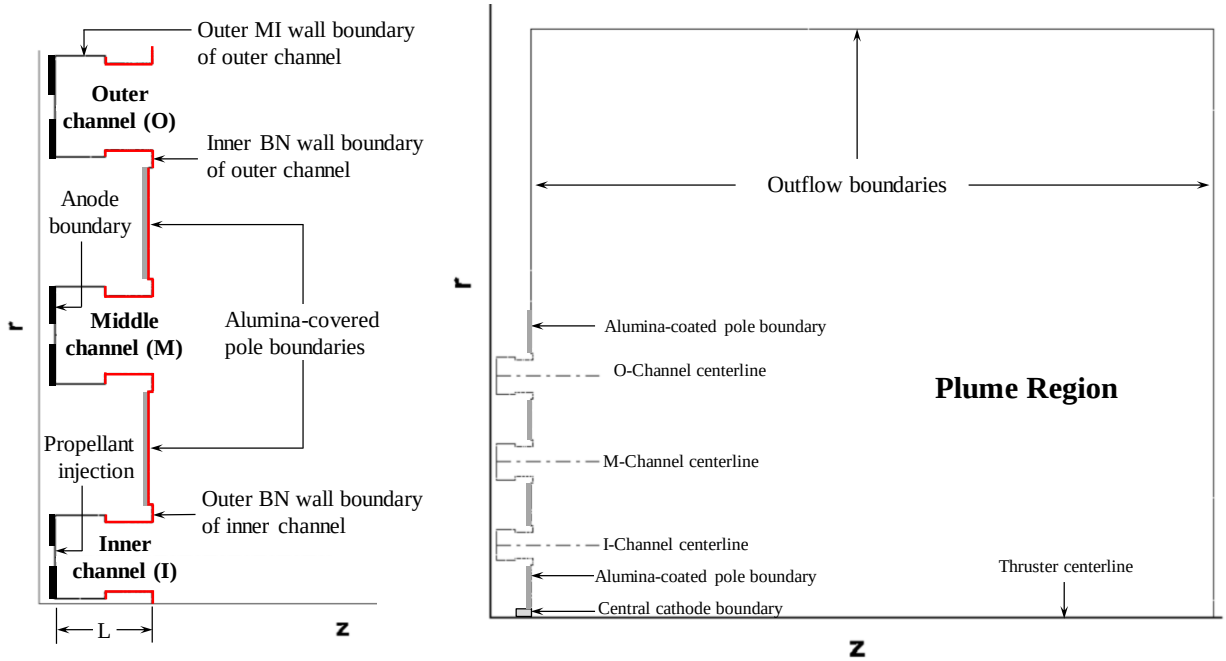

Fig 2. Schematic of the computational region for the X3 NHT simulations with Hall2De depicting relevant naming conventions used throughout this article. Left: Close-up view of the 3-channel arrangement. Black-outlined (—) boundaries are modeled as electrical conductors. Red-outlined (—) boundaries are electrical insulators. Right: The full computational domain showing far-plume BCs and the location of the cathode.

Compared to typical single-channel Hall thrusters, a unique computational challenge arose in the X3 due to the superposition of the magnetic field topologies associated with each of the three channels. Specifically, in the near-plume region a single magnetic null point is produced that prohibits in the MFAM discretization of the local region into single quadrilateral computational cells. Instead, due to the topology of the lines of force and their orthogonal set around the null point, an octalateral cell is formed as shown in Fig 3, which presents a challenge since all conservation laws in Hall2De are solved numerically using finite volume discretization that assumes each cell is formed by four sides (or edges). Since in this X3 arrangement only one null point is formed, the choice was made to re-discretize the single octalateral into three different quadrilateral cells as shown in Fig 3-right rather than generalizing Hall2De to allow for cells with >4 sides (a much more formidable task). The two dashed lines in Fig 3-right forming the center quadrilateral are assumed to be magnetic field lines and numerical fluxes across these edges are determined in the same manner as in any other magnetic edge. The addition of these

two new edges also leads however to 4 nodes around the center quadrilateral that are associated with 5 (instead of 4) edges. This is also problematic, in principle, since in Hall2De we assume $\leq$4 edges can be associated with each node. Since node variables however are only computed for visualization purposes from the primitive edge- or cell-centered variables, no changes were made to the code since the numerical solution remains unaffected.

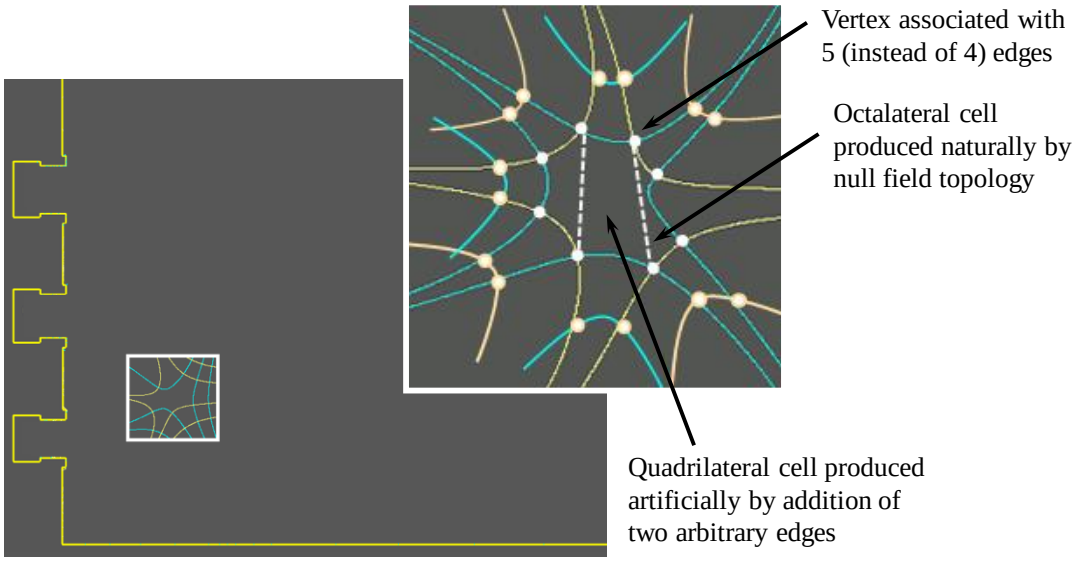

Fig 3. Numerical approach in the MFAM to produce quadrilateral computational cells out of the single octalateral cell created at a location in the plume region where the magnetic field topology has a null point. The null point is unique to the multi-channel arrangement and occurs due to the superposition of the single-channel topologies.

Table 1. Operating conditions and channel combinations simulated with the Hall2De code.

Channel(s) Operating			Discharge Power	Discharge Voltage	Discharge Current	Mass Flow Rate
I	M	O	(kW)	(V)	(A)	(mg/s)
✓	✓	✓	38	300	126.4	118.2
✓	✓	✓	49.6	400	124.6	122.1
✓			13	800	16.3	19.4
	✓		32	800	40.0	36.0
		✓	55	800	68.8	56.1
✓	✓	✓	100	800	125.0	95.5

The X3 was recently operated at the NASA Glenn Research Center (GRC) Vacuum Facility (VF) 5 at various conditions and channel combinations as reported in [12]. Specifically, the thruster demonstrated stable operation in all seven available channel combinations at discharge voltages ranging 300-500 V, three discharge currents ranging 16-247 A and total power ranging 5-102 kW. Each channel was designed to operate with approximately the same discharge current density (defined here as the ratio of the discharge current over the channel entrance area). However, the highest discharge voltage condition (800 V), which was the original focus of the numerical simulations was not tested. Therefore, to allow for direct comparisons with experiments, we have also conducted simulations at 300 V and 400 V for which the performance was measured during the tests at GRC. At these lower voltages, simulations were performed only when all three channels were operating at the same time. At 800 V some preliminary simulations

of each individual channel were conducted as a prelude to the full 3-channel operation. In this article, we present only results for the latter. Table 1 summarizes the operating conditions and channel combinations for which simulations were performed. The last column in Table 1 provides values for the total mass flow rate (anode + cathode). In the tests and simulations the percent cathode flow fraction, defined as the ratio of the cathode flow rate over the anode flow rate, was 7%.

III. Numerical Simulations

A. Plasma conditions and performance

Because Hall2De was not developed originally with the intent to allow for simulations of multiple-channel Hall thrusters, some minor code upgrades were required prior to commencing the work (in addition to handling the single octalateral cell discussed in the previous section). Most of the upgrades involved extending single-variable parameters in the code associated with a single channel to arrays, to allow for separate variable specifications in each channel. Obvious cases are the individual channel anode flow rates and the discharge currents. For example, for the discharge currents, the steady state value is specified in the code for each channel, based on either the intended thruster design or direct measurements. Then, what used to be a single-channel iteration on the magnitude of the anomalous collision frequency to obtain the discharge current is now a multiple-channel iteration. That is, iteration of the anomalous collision frequency for each channel is undertaken until the desired discharge currents are achieved. A typical evolution of the Hall2De solution for the channel discharge currents at the 300- and 400-V operating conditions is provided in Fig 4. The discharge voltage V_d, discharge current I_d and anode mass flow rate $\dot{m}_A$ for each channel as specified in Hall2De are listed in Table 2.

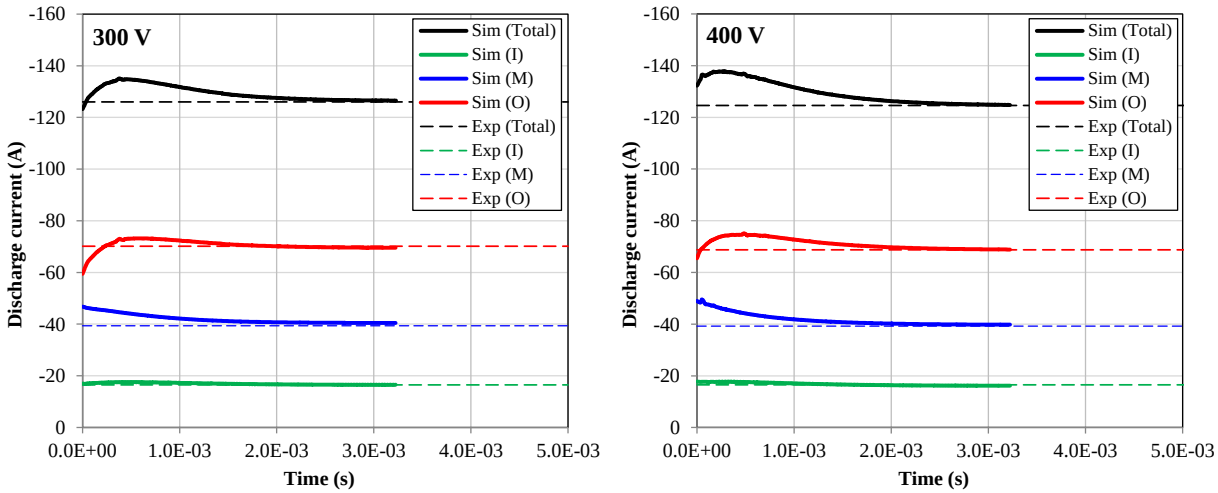

Fig 4. Typical evolution of the discharge currents during simulations at 300 V (left) and (400 V) of the X3 with all three channels operating. Values denoted "Exp" are those measured during the recent test campaign at NASA GRC [12] and are also listed in Table 2.

Also presented in the table are selected performance variables, thrust (T), anode specific impulse (Isp_A) and anode efficiency (ζ_A) to be discussed later in this section. The initial conditions for the solutions plotted in Fig 4 were specified based on previous simulations that were performed assuming VF5 conditions. Specifically, a backpressure of 4.75×10^{-6} Torr was assumed and a temperature of 500 C for the heavy species (neutrals and ions). No separate equation for the ion energy is solved in these simulations and therefore the ion temperature is assumed to be constant. The initial electron temperature and plasma potential were specified using generic spatial profiles based on experience of the typical gradients that are expected in these thrusters. The purpose of this (versus specifying fully-uniform conditions at time=0) is to accelerate the computation.

Table 2. Comparison between measurements ("Meas") and quantities that are either specified ("Spec") or computed ("Comp") in the simulations, for conditions in which all three channels are operating. Also indicated (by the symbol "•") are the contributions of each channel during the 3-channel operation. The measurements at 300 and 400 V were acquired during a recent test campaign at NASA GRC [12]. No measurements at 800 V were acquired during that campaign.

Channel Contribution			V_d (V)	I_d (A)		$\dot{m}_A$ (mg/s)		T (N)		Isp_A (s)		ζ_A (%)	
I	M	O		Spec	Meas	Spec	Meas	Comp	Meas	Comp	Meas	Comp	Meas
✓	✓	✓	300	126.4	126.0	118.2	118.7	2.16	2.37	1862	2040	51.9	62.6
•			300	16.5	16.5	17.1	13.7						
	•		300	40.4	39.4	39.7	40.0						
		•	300	69.5	70.1	61.4	64.9						
✓	✓	✓	400	124.6	124.6	122.1	122.1	2.64	2.77	2206	2312	57.2	63.3
•			400	16.2	16.5	17.1	15.6						
	•		400	39.7	39.3	40.6	41.0						
		•	400	68.7	68.8	64.5	65.4						
✓	✓	✓	800	125.4	N/A	95.5	N/A	3.17	N/A	3386	N/A	52.5	N/A
•			800	15.6	N/A	11.9	N/A						
	•		800	40.3	N/A	30.7	N/A						
		•	800	69.5	N/A	52.9	N/A						

Related to the iteration associated with the discharge currents is the specification of the anomalous collision frequency in the r-z plane. As mentioned in Sec. II.A, in numerical simulations the anomalous collision frequency ν_α is imposed in Hall2De using a so-called transport coefficient function f_α which defines the spatial variation along the channel centerline. Then ν_α is determined as follows:

$$\nu_a(z,r) = \gamma f_a(z,R_{CL})\omega_{ce}(z,R_{CL})\left[\frac{\omega_{ce}(z,R_{CL})}{\omega_{ce}(z,r)}\right]^{\delta}, \quad (1)$$

where (z,R_{CL}) denotes the axial location z along the channel centerline, located at radius R_{CL} relative to the thruster centerline. The numerical constant γ controls the magnitude of the frequency and is varied during the simulation until the specified discharge current is achieved. In the X3, γ is varied separately for each channel during the simulation until the individual channel discharge currents listed in Table 2 are achieved. The numerical constant δ is used to specify the

spatial dependence of the frequency on the magnetic field away from the centerline. In all simulations presented here δ=-1 which forces a linear dependence on |**B**|. In this multi-channel configuration an obvious question is where in the plume region does the model for ν_α associated with one channel cease and the model for the adjacent channel begin. For these first X3 simulations we have distinguished the plume regions as shown in Fig 5, where the separating boundaries are along the dashed lines shown in the figure, each of which starts at the midpoint of the pole boundary between two channels. This approach at first may seem that it can potentially lead to discontinuities across these fictitious boundaries. However, as will be shown shortly, the anomalous frequency reaches its maximum value of ω_{ce} near the channel exit so most of the plume is dominated by this value. Therefore the collision frequency remains continuous in these regions of the thruster. The subscripts I, M, and O in Fig 5 for ν_α correspond to the channel with which it is associated.

Typically, the specification of f_α has been guided by plasma measurements whenever they exist. In the X3 however no internal or near-plume measurements exist. Thus, function f_α has been defined based on previous work with the unshielded version of the 6-kW laboratory Hall thruster H6 for which both detailed simulations and plasma measurements exist. This means that the results presented herein are subject to a higher uncertainty than those for which direct plasma measurements exist since, despite some similarities of the individual channels and magnetic field in the X3 with those in the H6, the precise variation of f_α is not known. Moreover, though we will be discussing comparisons with the thruster's measured performance (Table 2) in ensuing sections, such comparisons provide some idea about our uncertainties but do not provide sufficient information to allow for rigorous validation of the simulations.

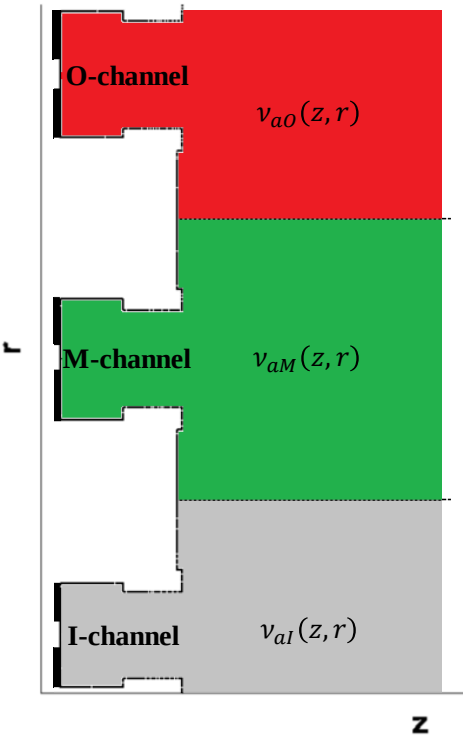

Fig 5. Regions associated with each acceleration channel and the model of the anomalous collision frequency employed in the Hall2De simulations.

The steady-state anomalous and classical collision frequencies due to electron-ion (e-i) and electron-neutral (e-n) interactions are plotted in Fig 6-right for the 300-, 400- and 800-V operating conditions when all three channels are operating. The channel centerline solutions for the electron temperature and plasma potential are plotted in Fig 6-left. The dominance of the total collision frequency by the anomalous contribution over the classical in the acceleration and near plume regions that occurs in most modern single-channel Hall thrusters is evident here as well, for all channels of the X3 and all discharge voltages we simulated. The computed maximum electron temperature is found to be approximately 12-15% of the discharge voltage at 300 and 400 V. The range is slightly higher at 800 V, 14-16%. These values are somewhat higher than what is typically observed in single-channel thrusters but not unreasonably high. The computed temperature values may also be different if the true anomalous collision frequency is different than that assumed by the model, especially regarding its axial location since this largely determines the location of the acceleration region.

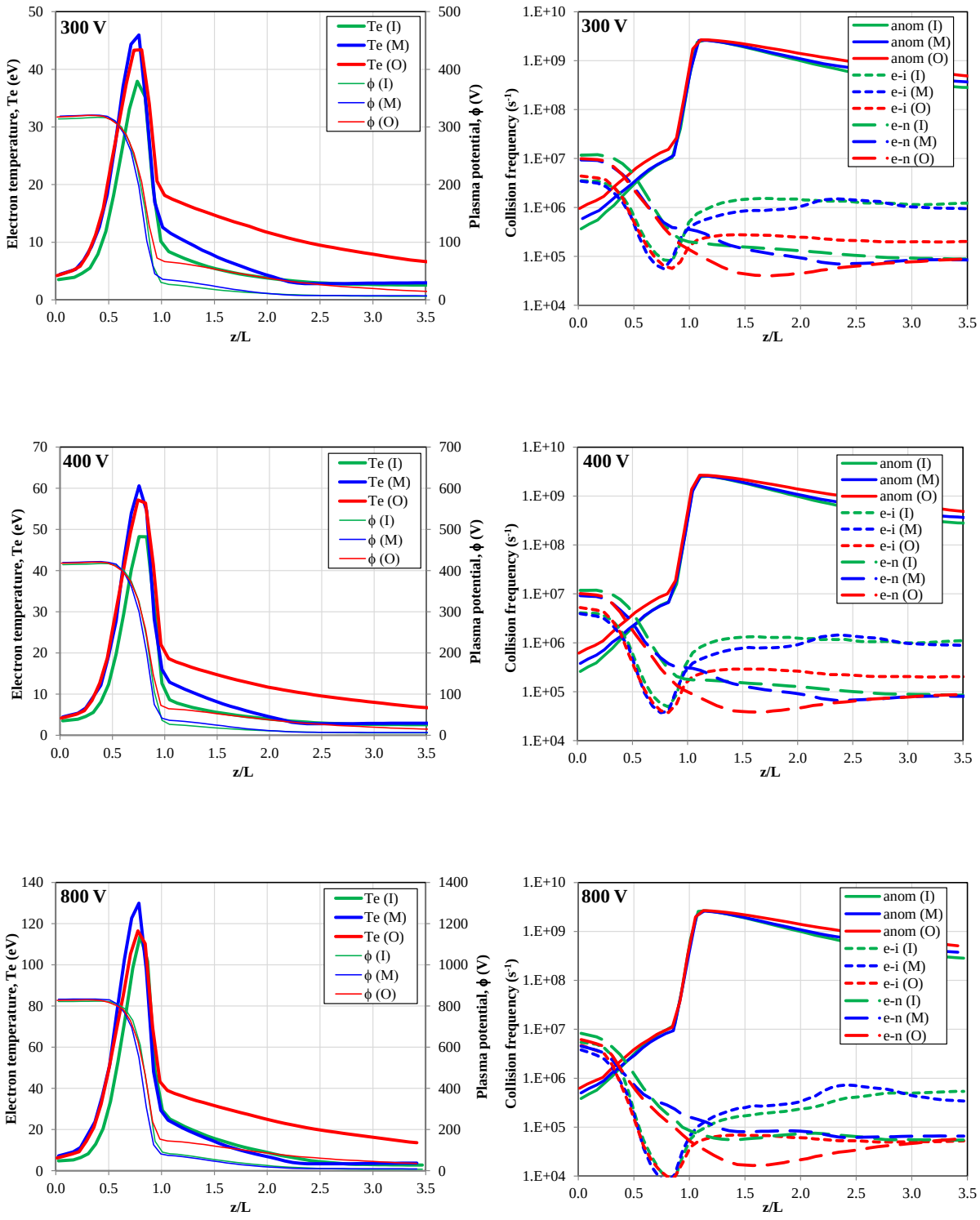

Fig 6. Computed results along the centerline of each channel from Hall2De simulations of the X3 with all three channels operating, at 300 V (top), 400 V (middle) and 800 V (bottom). Left column: Plasma potential (ϕ) and electron temperature (T_e). Right column: electron collision frequencies.

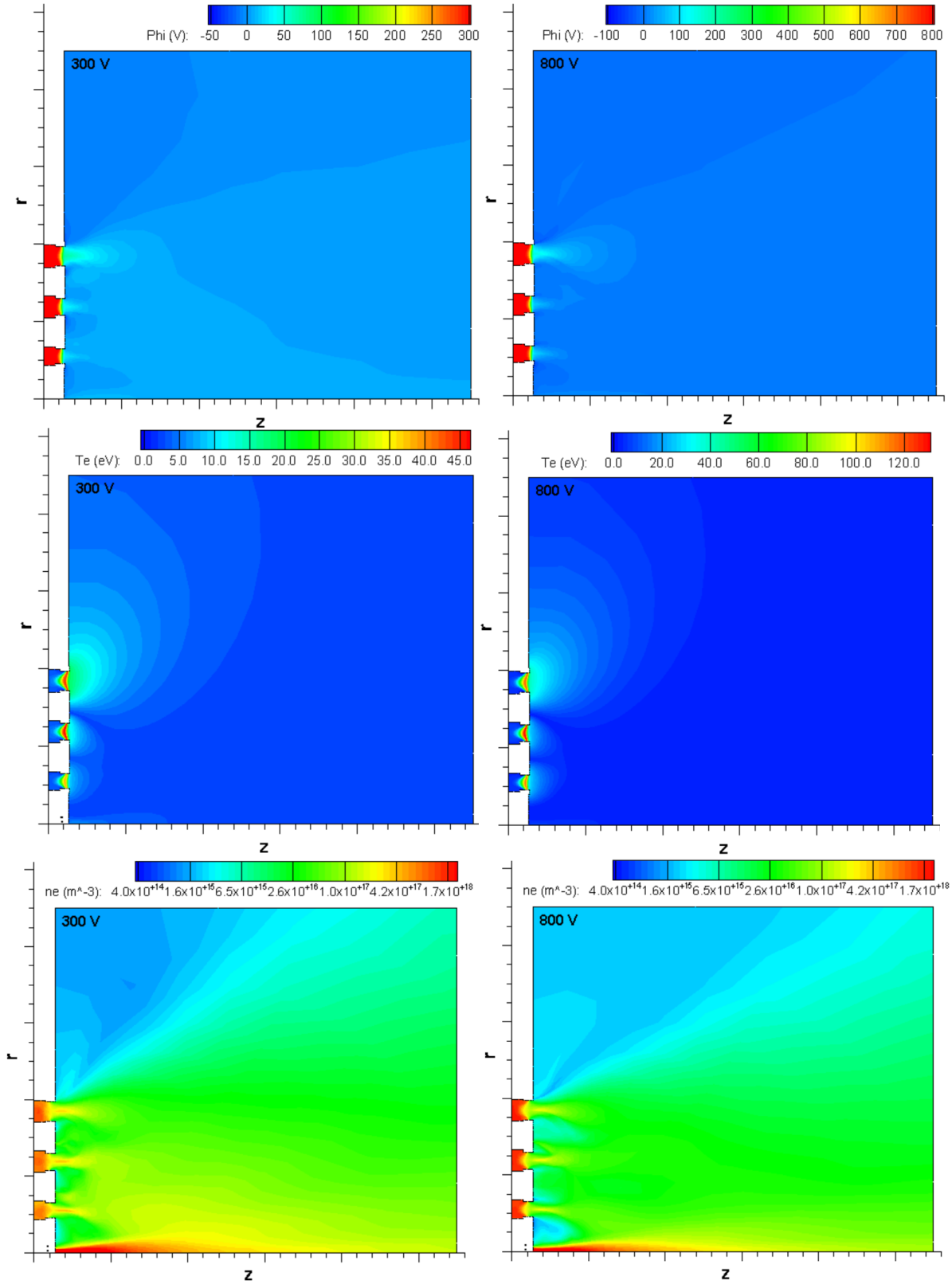

Fig 7. Contour plots from Hall2De simulations of the X3 with all three channels operating, at discharge voltages of 300 V (left column) and 800 V (right column). Top: plasma potential. Middle: electron temperature. Bottom: electron number density.

Also evident in the simulations is that for all discharge voltages the maximum electron temperature is lower in the inner channel compared to that in the other two channels. For the outer channel, the temperature is comparable to that in the middle channel at 300 V and 400 V whereas it is comparable to that in the inner channel at 800 V. This comparison between outer or middle and inner channels occurs despite the fact that the discharge current density is designed to be approximately the same in each channel. In fact a closer examination of the results at 300 V for example reveals that the major source of electron heating, namely the work done by the electric field (mathematically expressed as $\mathbf{E}\cdot\mathbf{j}_e$ where $\mathbf{E}$ is the electric field and $\mathbf{j}_e$ is the electron current density), is indeed comparable in the outer and inner channels at the location of maximum heating. This is expected since both the discharge current density and the plasma potential along the channel centerline are approximately the same as illustrated in Fig 6-left. This then implies that the rate associated with one or more cooling mechanisms for electrons must be higher in the inner channel. Indeed, we find that the ionization losses in the inner channel are approximately 70% higher than those in the outer channel, which is largely due to the specified anode flow rate (Table 2). Taking into consideration the channel area, the specified anode flow rate in the inner channel produces higher flux of neutrals than in the outer channel and, in turn, higher neutral gas density and ionization rates. We note that in the recent tests at NASA GRC, the operating flow rate at 300 V was approximately 25% lower than the value specified in the simulations for the inner channel, and 5.4% higher for the outer channel. This is sufficient to reverse the trend making the neutral flux higher in the outer channel (by a little over 10%) compared to that in the inner channel. We postulate therefore that either higher or comparable electron temperatures may had been produced during the tests inside the inner channel compared to those in the outer channel. As noted earlier, the flow rates specified in the simulations were based on original X3 design estimates and are different than those in the GRC tests. We therefore plan to repeat the simulations using the values measured during the GRC tests since there was not sufficient time to do so prior to the writing of this paper.

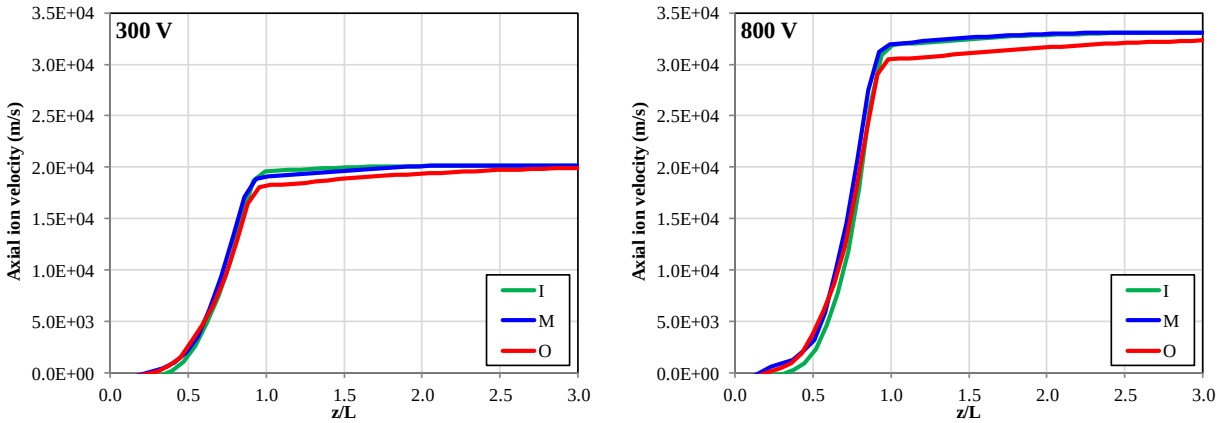

Fig 8. Computed axial velocity of singly-charged ions along the centerline of each channel from Hall2De simulations of the X3 with all three channels operating, at discharge voltages of 300 V (left) and 800 V (right).

Fig 7 shows contour plots of the plasma potential (top), electron temperature (middle) and electron number density, n_e, (bottom), at 300 V (left column) and 800 V (right column). The simulation results correspond to the specified steady-state discharge currents and anode flow rates provided in Table 2. Noted are the higher plasma potentials and electron temperatures in the plume of the outer channel compared to the other two channels. This trend was also evident in

the channel centerline plots of Fig 6, by the comparisons downstream of z/L~1. One of the consequences of the elevated plume plasma potential is that ions are accelerated through a smaller potential difference as they exit the channel and therefore their exhaust velocity there is less. This is better shown in Fig 8 which plots the computed axial velocity of singly-charged ions at 300 V and 800 V. In both cases further acceleration of ions does occur in the outer channel plume but it takes at least three channel lengths to achieve the same velocity as that at the inner channel exit.

The applied magnetic field appears to be the driving source behind the elevated electron temperatures and, in turn, plasma potentials in the near plume of the outer channel. In Fig 9 we plot the ratio of the radial component of the magnetic field over the maximum value, $B_r/|B_{r,max}|$ in the near-plume region, along the centerline of each of the three channels. A comparison of the three profiles clearly shows a higher magnetic field in the plume of the outer channel than that in the other two channels. This then means that the resistivity of the plasma, η, also is higher since, in this region of the outer channel, $\nu_\alpha=\omega_{ce}$ and hence $\eta\sim|B|/n_e$. A higher resistivity also implies higher resistive heating of the electrons (ηj_e^2) which explains the elevated electron temperatures found in the plume of the outer channel (Figs 6 and 7). Electron heating is then accompanied by an increase in the plasma potential as well through the electron pressure. The electron number density (Fig 6-bottom) is found not to be a significant contributor to the differences in the pressure. We note that without the electron pressure gradient in Ohm's law, a higher resistivity would only yield a lower (not higher) potential in this region. It therefore appears there is room for further optimization of the applied magnetic field in this region of the thruster that can reduce electron heating and improve ion acceleration.

Thrust, anode specific impulse and anode efficiency are computed as follows in Hall2De:

$$T = \sum_{i_E}^{N_E}\sum_{i_Z=1}^{N_Z}\sum_{i_F=1}^{N_F}\left(mu\boldsymbol{\Gamma} + p\right)_{i_E,i_Z,i_F}\cdot d\mathbf{S}_{i_E}$$
$$Isp_A = \frac{T}{\dot{m}_A g} \qquad \zeta_A = \frac{T^2}{2\dot{m}_A P_d}, \tag{2}$$

where the mass, axial component of the velocity, flux vector and pressure of the ion are given by m, u, $\boldsymbol{\Gamma}$ and p, respectively. The thrust is determined by integration along a plume magnetic field line that is made up by N_E number of computational edges, with each edge that contributes to the sum denoted by i_E. The surface area of each edge is S_{iE}. The contributions from all ion charge states N_Z and fluid states N_F are accounted for by summing over each individual charge and fluid state i_Z and i_F, respectively. Since no measurements in the recent GRC tests were performed at 800 V, we present in Table 2 comparisons between computed and measured values at 300 and 400 V only. The simulations under-predict the experimental values at both discharge voltages with the highest discrepancy occurring at 300 V. Specifically, T, Isp_A and ζ_A are under-predicted at 300 V by 9.1%, 8.7% and 17.1%, respectively whereas the corresponding values at 400 V are 4.6%, 4.6% and 9.6%. The discrepancies at 300 V are larger than typical Hall2De simulations and the reason is twofold. First, the precise location of the ionization and acceleration zones is not known as accurately as in other thrusters in which plasma measurements have helped guide the anomalous collision frequency. Differences of a few millimeters in this location can change the computed performance by at least a few %. Second, and likely the largest contributor to the discrepancy, are the differences between the specified and measured anode mass flow rates for

each individual channel. As mentioned earlier the values specified in the simulations were based on thruster design and limited test data acquired prior to the more extensive test campaign at GRC the results of which became available only shortly before the writing of this paper. More specifically, compared to the measured value at GRC the anode flow rate in the simulation was 24.8% higher for the inner channel and 5.4% lower for the outer channel. Since the contribution to the thrust by the outer channel is much greater than that by the inner channel, the error in the computed thrust is exacerbated. By contrast, the flow discrepancies are smaller at 400 V, namely 9.6% higher for the inner channel and 1.4% lower for the outer channel, which yield also better agreement between computed and measured performance. Of course, the worst comparison at both discharge voltages is for the anode efficiency since it is proportional to the square of the thrust. New simulations that specify the values measured in the GRC tests are planned for the near future.

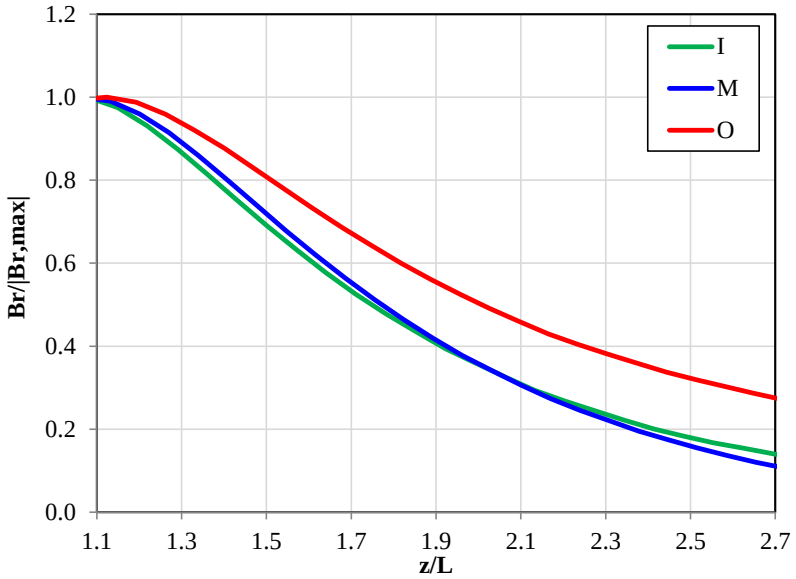

Fig 9. Variation of the radial component of the applied magnetic field (B_r) over the maximum value ($B_{r,max}$) along the centerline of each channel's plume region.

B. **Channel Erosion**

Erosion in Hall2De accounts for contributions from up to three charge states, Xe^{+}, Xe^{++} and Xe^{+++}, and up to four ion fluids. The sputtering erosion rate (ε) due to ion bombardment by ions is given by,

$$\varepsilon_{i_Z,i_F} = j_{i_Z,i_F} Y \tag{3}$$

where the incident ion current density perpendicular to the channel wall is denoted as j_{i_Z,i_F}. The sputtering yield of the channel material, Y, is a function of the ion impact energy K and incidence angle β. The total erosion rate is the sum over all fluids and all charge states:

$$\varepsilon = \sum_{i_Z=1}^{N_Z} \sum_{i_F=1}^{N_F} \varepsilon_{i_Z,i_F} \ . \tag{4}$$

Because ions must traverse a sheath before striking the wall, the total impact energy is the sum of the kinetic energy ions have acquired in the plasma upon entrance to the sheath, and the sheath potential energy. The potential energy, transformed to ion kinetic energy as the plasma ions are accelerated inside the sheath towards the solid material, is computed based on the Hobbs and Wesson solution to the 1-D sheath equations in the presence of secondary electron emission [32]. In the numerical simulations the edge-centered ion velocity and the element-centered ion number density at each computational element adjacent to the wall boundary are used to determine the total impact energy, $K=K_{plasma}+ K_{sheath}$, and angle β. Then the sputtering yield is determined as follows:

$$Y = f_\beta(\beta) f_K(K) \tag{5}$$

where $f_\beta(\beta)$ and $f_K(K)$ are fitting functions for the angle and energy dependence at zero angle of incidence, respectively. For BN, we have been using a model by Bohdansky [33] to extrapolate Y from the available data at K>100 V to lower ion energies. The fitting functions we have used are as follows:

$$f_\beta(\beta) = \cos(\beta)^{-c_0} \exp\left[-c_1\left(\cos(\beta)^{-c_2} - 1\right)\right] \qquad f_K(K) = A'\left(1-\frac{K_T}{K}\right)^2\left(1-\left(\frac{K_T}{K}\right)^{2/3}\right). \tag{6}$$

The coefficients in Eq (6) used for the channel walls in the X3 are provided in [23] where the reader will also find plots of the functions for BN. In Hall2De, ε is set to zero when the ion energy is less than the threshold value, K_T.

The computed erosion rates along the inner and outer walls of all three channels, at 300 V and 800 V, are depicted in Fig 10. Since the X3 does not employ magnetic shielding the erosion patterns and values resemble those found in other unshielded thrusters like the H6US (e.g. see [34, 35]). Specifically, we find that the erosion peaks in the acceleration region ($z/L \gtrsim 0.8$) for all three channels to values in the order of 10^{-3} mm/h (10^3 μm/kh) at 300 V (Fig 10-left) and to ~3× higher than that at 800 V (Fig 10-right). By way of comparison, at a discharge power of 6 kW the discharge current density in the H6US is 2.2× that in the X3 inner channel when both thrusters are operating at 300 V. The maximum erosion rate (averaged over all rings) was found to be about 8.5× higher in the H6US, 8.5×10^{-3} mm/h (8.5×10^3 μm/kh).[34, 35] The precise value and location of the maximum erosion is dependent upon the location of the acceleration zone which is dependent upon the modeled spatial profile of the anomalous collision frequency. Since the latter has not yet been fully validated in the X3 by plasma measurements, our uncertainty regarding this location is higher than that in the H6US and can be as much as several millimeters. This could change also the computed value of the maximum erosion in the X3 by a factor of two or less. For reference, when all three channels are operating in the X3 at 300 V, the discharge power and current associated with the inner channel are about 5 kW and 16.5 A, respectively. For the middle channel the corresponding values are 12.1 kW and 40.4 A (Table 2 and [12]).

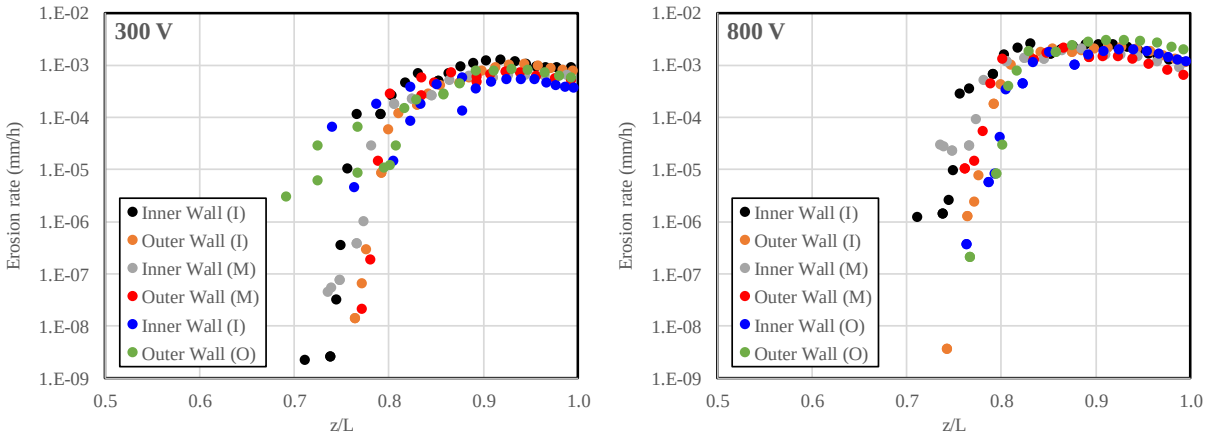

Fig 10. Computed erosion rates along the inner and outer walls of the X3 when all three channels are operating at 300 V (left) and 800 V (right).

IV. Conclusions

The first successful numerical simulations of a 3-channel NHT using Hall2De have demonstrated the code's promise to support the design and service life qualification of Hall thruster technologies beyond just those operating with a single acceleration channel. With relatively minimal code upgrades, these first Hall2De simulations of the X3 NHT focused on operation with all three channels firing at discharge voltages of 300, 400 and 800 V and provided preliminary performance and channel erosion predictions. Because the performance data from a recent extensive experimental campaign at NASA GRC did not become available in time to repeat the X3 simulations already completed using somewhat different flow rate conditions for each channel, direct one-on-one comparisons were not possible. However, in one case studied, namely 400 V and 49.6 kW, in which the anode flow rates were the closest between simulation and experiment, the performance values were found to be within 5% of each other for the thrust and anode specific impulse and within 10% for the anode efficiency. A closer examination of the Hall2De solution for the plasma showed elevated electron temperature and plasma potential in the near-plume region of the outer channel compared to values computed near the other two channels. We argued this was the consequence of the magnetic field design which employs slightly higher strength in the near-plume of the outer channel compared to the other channels. This then increases resistive heating in the region. As a result of the elevated plasma potential, ion acceleration persists further downstream than in the other two channels. Therefore some additional optimization of the magnetic field in this region of the outer channel may be possible.

The Hall2De simulations have also allowed for the first estimates of the erosion rates along the (BN) channel walls of the X3. We compute values in the order of 10^{-3} mm/h (10^{3} m/kh) at 300 V when all channels are operating. At 10^{-3} mm/h no more than 10 mm of the BN is expected to erode away by ion sputtering after 10,000 h, the design goal for thruster operational life of the XR-100 system. The channel erosion rates in the X3 at 800 V were a few times higher than those at 300 V.

In the absence of plasma measurements in the near-plume and acceleration channels, and with only limited performance measurements produced by different conditions than those specified in the simulations, it should be acknowledged that the results produced by this first series of simulations of an NHT are subject to a higher uncertainty than Hal2De simulations of single-channel thrusts (like the H6) for which more data was available. With the performance data from the recent campaign at NASA GRC now fully available, the next series of Hall2De simulations

will aim at specifying the exact conditions employed during those tests to allow for a more rigorous validation of the code predictions and to assess the sensitivity of the computed results on critical assumptions such as those associated with anomalous collision frequency model.

Acknowledgments

The support of the collaborative effort between Aerojet Rocketdyne, UM, JPL and NASA GRC by NASA's NextSTEP program is gratefully acknowledged. The authors also wish to thank Scott Hall and Sarah Cusson for providing the applied magnetic field, thruster geometry and materials, as well as operating conditions and performance data for the X3 simulations. Portions of the research described in this paper were carried out at the Jet Propulsion Laboratory, California Institute of Technology, under a contract with the National Aeronautics and Space Administration.

References

[1] S. J. Hall, A. D. Gallimore, H. Kamhawi, D. Brown, J. E. Polk, D. M. Goebel, and R. R. Hofer, "Implementation and Initial Validation of a 100-kW Class Nested-channel Hall Thruster," in 50th AIAA/ASME/SAE/ASEE Joint Propulsion Conference, Cleveland, OH, AIAA-2014-3815, July 2014.

[2] S. J. Hall, S. E. Cusson, and A. D. Gallimore, "30-kW Performance of a 100-kW Class Nested-Channel Hall Thruster," in 34th International Electric Propulsion Conference, Hyogo-Kobe, Japan, IEPC-2015-125, July 2015.

[3] R. Florenz, S. J. Hall, A. D. Gallimore, H. Kamhawi, C. Griffiths, D. Brown, R. R. Hofer, and J. E. Polk, "First Firing of a 100-kW Nested-channel Hall Thruster," in 33rd International Electric Propulsion Conference, Washington, DC, IEPC-2013-394, October 2013.

[4] R. Liang, and A. D. Gallimore, "Performance of a Laboratory Hall Thruster with Two Concentric Discharge Channels," in 57th JANNAF Propulsion Meeting, 7th Modeling and Simulation, 5th Liquid Propulsion, 4th Spacecraft Propulsion, Joint Subcommittee Meeting, Colorado Springs, CO, 2010.

[5] L. Mason, R. Jankovsky, and D. Manzella, "1000 hours of testing on a 10 kilowatt Hall effect thruster," *37th Joint Propulsion Conference and Exhibit*, Joint Propulsion Conferences: American Institute of Aeronautics and Astronautics, 2001.

[6] R. Jankovsky, D. Jacobson, C. Sarmiento, L. Pinero, D. Manzella, R. Hofer, and P. Peterson, "NASA's Hall Thruster Program 2002," *38th AIAA/ASME/SAE/ASEE Joint Propulsion Conference & Exhibit*, Joint Propulsion Conferences: American Institute of Aeronautics and Astronautics, 2002.

[7] D. Manzella, R. Jankovsky, and R. Hofer, "Laboratory Model 50 kW Hall Thruster," *38th AIAA/ASME/SAE/ASEE Joint Propulsion Conference & Exhibit*, Joint Propulsion Conferences: American Institute of Aeronautics and Astronautics, 2002.

[8] D. Jacobson, D. Manzella, R. Hofer, and P. Peterson, "NASA's 2004 Hall Thruster Program," *40th AIAA/ASME/SAE/ASEE Joint Propulsion Conference and Exhibit*, Joint Propulsion Conferences: American Institute of Aeronautics and Astronautics, 2004.

[9] P. Peterson, D. Jacobson, D. Manzella, and J. John, "The Performance and Wear Characterization of a High-Power High-Isp NASA Hall Thruster," *41st AIAA/ASME/SAE/ASEE Joint Propulsion Conference & Exhibit*, Joint Propulsion Conferences: American Institute of Aeronautics and Astronautics, 2005.

[10] I. G. Mikellides, and I. Katz, "Numerical simulations of Hall-effect plasma accelerators on a magnetic-field-aligned mesh," *Physical Review E*, vol. 86, no. 4, pp. 046703, Oct 17, 2012.

[11] I. Katz, and I. G. Mikellides, "Neutral gas free molecular flow algorithm including ionization and walls for use in plasma simulations," *Journal of Computational Physics,* vol. 230, no. 4, pp. 1454-1464, Feb 20, 2011.
[12] S. J. Hall, B. A. Jornsy, A. D. Gallimore, H. Kamhawi, T. W. Haag, J. A. Mackey, W. Huang, J. H. Gilland, and P. Y. Peterson, "High-Power Performance of a 100-kW Class Nested Hall Thruster," in 35th International Electric Propulsion Conference, Atlanta, GA, IEPC-2017-228, October 2017.
[13] A. Lopez Ortega, and I. G. Mikellides, "A New Cell-Centered Implicit Numerical Scheme for Ions in the 2-D Axisymmetric Code Hall2De," in 50th AIAA/ASME/SAE/ASEE Joint Propulsion Conference, Cleveland, OH, AIAA-2014-3621, July 2014.
[14] I. G. Mikellides, I. Katz, and R. R. Hofer, "Design of a Laboratory Hall Thruster with Magnetically Shielded Channel Walls, Phase I: Numerical Simulations," in 47th AIAA/ASME/SAE/ASEE Joint Propulsion Conference, San Diego, CA, AIAA-2011-5809, July 2011, pp. 5809.
[15] I. G. Mikellides, I. Katz, R. R. Hofer, and D. M. Goebel, "Design of a Laboratory Hall Thruster with Magnetically Shielded Channel Walls, Phase III: Comparison of Theory with Experiment," in 48th AIAA/ASME/SAE/ASEE Joint Propulsion Conference, Atlanta, GA, AIAA-2012-3789, July 2012.
[16] N. B. Meezan, W. A. Hargus, and M. A. Cappelli, "Anomalous electron mobility in a coaxial Hall discharge plasma," *Physical Review E,* vol. 63, no. 2, pp. 026410, Feb, 2001.
[17] A. Ducrocq, J. C. Adam, A. Heron, and G. Laval, "High-frequency electron drift instability in the cross-field configuration of Hall thrusters," *Physics of Plasmas,* vol. 13, no. 10, Oct, 2006.
[18] A. Lazurenko, T. D. de Wit, C. Cavoit, V. Krasnoselskikh, A. Bouchoule, and M. Dudeck, "Determination of the electron anomalous mobility through measurements of turbulent magnetic field in Hall thrusters," *Physics of Plasmas,* vol. 14, no. 3, Mar, 2007.
[19] C. Boniface, L. Garrigues, G. J. M. Hagelaar, J. P. Boeuf, D. Gawron, and S. Mazouffre, "Anomalous cross field electron transport in a Hall effect thruster," *Applied Physics Letters,* vol. 89, no. 16, Oct 16, 2006.
[20] J. C. Adam, A. Heron, and G. Laval, "Study of stationary plasma thrusters using two-dimensional fully kinetic simulations," *Physics of Plasmas,* vol. 11, no. 1, pp. 295-305, Jan, 2004.
[21] P. Coche, and L. Garrigues, "A two-dimensional (azimuthal-axial) particle-in-cell model of a Hall thruster," *Physics of Plasmas,* vol. 21, no. 2, Feb, 2014.
[22] I. G. Mikellides, A. L. Ortega, I. Katz, and B. A. Jorns, "Hall2De Simulations with a First-principles Electron Transport Model Based on the Electron Cyclotron Drift Instability," in 52nd AIAA/ASME/SAE/ASEE Joint Propulsion Conference, Salt Lake City, UT, July 2016.
[23] A. Lopez Ortega, I. G. Mikellides, and V. H. Chaplin, "Numerical Simulations for the Assessment of Erosion in the 12.5-kW Hall Effect Rocket with Magnetic Shielding (HERMeS)," in 35th International Electric Propulsion Conference, Atlanta, GA, IEPC-2017-154, October 2017.
[24] J. C. Butcher, "Numerical methods for ordinary differential equations in the 20th century," *Journal of Computational and Applied Mathematics,* vol. 125, no. 1-2, pp. 1-29, Dec 15, 2000.
[25] A. Lopez Ortega, I. G. Mikellides, and I. Katz, "Hall2De Numerical Simulations for the Assessment of Pole Erosion in a Magnetically Shielded Hall Thruster," in 34th International Electric Propulsion Conference, Hyogo-Kobe, Japan, IEPC-2015-249, July 2015.
[26] I. Katz, A. Lopez Ortega, D. M. Goebel, M. J. Sekerak, R. R. Hofer, B. A. Jorns, and J. R. Brophy, "Effect of Solar Array Plume Interactions on Hall Thruster Cathode Common Potentials," in 14th Spacecraft Charging Technology Conference, ESA/ESTEC, Noordwijk, NL, 2016.
[27] P. Y. Peterson, H. Kamhawi, W. Huang, G. Williams, J. H. Gilland, J. Yim, R. R. Hofer, and D. A. Herman, "NASA's HERMeS Hall Thruster Electrical Configuration Characterization," *52nd*

AIAA/SAE/ASEE Joint Propulsion Conference, AIAA Propulsion and Energy Forum: American Institute of Aeronautics and Astronautics, 2016.

[28] R. R. Hofer, J. E. Polk, M. J. Sekerak, I. G. Mikellides, H. Kamhawi, T. Verhey, D. Herman, and G. Williams, "The 12.5 kW Hall Effect Rocket with Magnetic Shielding (HERMeS) for the Asteroid Redirect Robotic Mission," in 52nd AIAA/ASME/SAE/ASEE Joint Propulsion Conference, Salt Lake City, UT., AIAA-2016-4825, 2016.

[29] G. D. Hobbs, and J. A. Wesson, "Heat Flow through a Langmuir Sheath in Presence of Electron Emission," *Plasma Physics,* vol. 9, no. 1, pp. 85-87, 1967.

[30] I. G. Mikellides, I. Katz, D. M. Goebel, and J. E. Polk, "Hollow cathode theory and experiment. II. A two-dimensional theoretical model of the emitter region," *Journal of Applied Physics,* vol. 98, no. 11, Dec 1, 2005.

[31] I. G. Mikellides, D. M. Goebel, J. S. Snyder, I. Katz, and D. A. Herman, "The discharge plasma in ion engine neutralizers: Numerical simulations and comparisons with laboratory data," *Journal of Applied Physics,* vol. 108, no. 11, Dec 1, 2010.

[32] R. R. Hofer, I. G. Mikellides, I. Katz, and D. M. Goebel, "AIAA Paper No. 07-5267," in Proceedings of the 43rd AIAA Joint Propulsion Conference, Cincinnati, OH, 2007, pp. 5267.

[33] J. Bohdansky, "A Universal Relation for the Sputtering Yield of Monatomic Solids at Normal Ion Incidence," *Nuclear Instruments & Methods in Physics Research Section B-Beam Interactions with Materials and Atoms,* vol. 2, no. 1-3, pp. 587-591, 1984.

[34] R. R. Hofer, D. M. Goebel, I. G. Mikellides, and I. Katz, "Magnetic shielding of a laboratory Hall thruster. II. Experiments," *Journal of Applied Physics,* vol. 115, no. 4, Jan 28, 2014.

[35] I. G. Mikellides, I. Katz, R. R. Hofer, and D. M. Goebel, "Magnetic shielding of a laboratory Hall thruster. I. Theory and validation," *Journal of Applied Physics,* vol. 115, no. 4, Jan 28, 2014.